



严重急性呼吸综合征冠状病毒2 JN.1 变异株对广谱中和抗体的免疫逃逸机制研究*

谢佳雯¹⁾ 刘天赐²⁾ 郭梦甜²⁾ 冯璐璐²⁾ 孙铭辰²⁾ 刘攀²⁾ 朱谦慧^{2) **}

(¹) 北京师范大学生命科学学院, 北京 100875; ²) 中国科学院生物物理研究所生物大分子全国重点实验室, 北京 100101)

摘要 目的 随着严重急性呼吸综合征冠状病毒2 (SARS-CoV-2) Omicron 亚型的持续进化, 尤其是 BA.2.86 及其子代 JN.1 的出现, 给现有中和抗体的防控策略带来了严峻挑战。本研究旨在阐明 JN.1 变异株对广谱中和抗体的免疫逃逸机制, 为广谱疫苗与中和抗体药物的理性设计提供了重要的结构指导。**方法** 通过生物膜层干涉技术 (bio-layer interferometry, BLI), 系统评估三株先前筛选获得的广谱中和抗体 (XGv074、XGv302、XGv303) 对 BA.2.86 及 JN.1 变异株的结合与中和能力; 利用冷冻电镜解析 BA.2.86 刺突蛋白 (Spike, S) 三聚体与 XGv074、XGv302 及 XGv303 抗原结合片段 (fragment of antigen binding, Fab) 的复合物结构; 结合分子动力学模拟和结合自由能分解, 分析关键突变对抗体结合的影响。**结果** XGv074、XGv302 和 XGv303 对 BA.2.86 仍保持中和活性, 但对 JN.1 的结合能力显著降低, 仅 XGv074 保留微弱中和活性。结构分析表明, JN.1 的 L455S 突变破坏了 XGv302 与受体结合域 (receptor binding domain, RBD) 之间的关键疏水相互作用, 导致抗体逃逸。结合自由能分解进一步揭示 L455 和 Y421 为能量热点残基, L455S 突变直接削弱了抗体结合。XGv074 因重链互补决定区 3 (heavy chain complementarity-determining region 3, HCDR3) 构象柔性较高, 部分耐受突变。**结论** JN.1 通过 RBD 区关键位点突变逃逸广谱中和抗体, 其机制涉及能量热点破坏和抗体结合界面重构。抗体的构象柔性可能增强其对突变的适应性, 本研究为广谱疫苗和抗体设计提供了重要指导, 强调了表位能量热点和抗体柔性结构在维持中和广谱性中的重要作用。

关键词 SARS-CoV-2, BA.2.86, JN.1, 中和抗体, 冷冻电镜, 中和机制, 逃逸机制

中图分类号 Q937

DOI: 10.3724/j.pibb.2025.0336

CSTR: 14.32369.pibb.20250336

随着严重急性呼吸 (severe acute respiratory syndromes-coronary virus 2, SARS-CoV-2) 的持续进化, 新兴变异株不断通过积累 Spike 突变实现对免疫系统的逃逸。从 2024 年底至 2025 年初, JN.1 毒株凭借其显著增强的传播能力和免疫逃逸特性, 迅速成为全球主导流行株, 并被世界卫生组织 (World Health Organization, WHO) 列为“需要关注的变异株” (variant of interest, VOI)^[1]。Spike 按功能可分为 S1 和 S2 两个亚基, 分别负责识别宿主细胞受体及介导病毒与宿主细胞膜的融合。S1 亚基进一步可细分为 4 个结构域, 包括 N 端结构域 (N-terminal domain, NTD)、受体结合域 (receptor binding domain, RBD)、亚结构域 1

(subdomain 1, SD1) 和亚结构域 2 (subdomain 2, SD2), 其中 RBD 不仅直接介导与人血管紧张素转换酶 2 (human angiotensin-converting enzyme 2, hACE2) 受体的结合^[2], 而且同时是诱导产生大多数中和抗体的主要区域。与引起 2023 年上半年全球大流行的新冠变异株 XBB.1.5 相比, JN.1 的 S 蛋白上有 36 个位点的突变或缺失, 其中有 13 个位点位于 RBD 上。而 JN.1 与其父代流行株 BA.2.86 相比, 在 RBD 上新积累了一个突变

* 国家重点研发计划 (2018YFA0900801) 资助项目。

** 通讯联系人。

Tel: 010-64889939, E-mail: zhuanhui@ibp.ac.cn

收稿日期: 2025-07-15, 接受日期: 2025-08-18

L455S，导致疫苗的保护效果和中和抗体药物的治疗效果进一步降低^[3-4]。因此，深入解析JN.1的免疫逃逸机制，对于下一代广谱疫苗和中和抗体的设计具有重要意义。

在之前的研究中，本课题组筛选出一组靶向RBD ($n=19$) 的单克隆抗体对SARS-CoV-2 D614G 和 omicron 代表性亚系 (BA.1、BA.2、BA.5、BA.2.75) 表现出广泛而有效的中和活性^[5]。然而，针对BA.2.86变异株，仅有XGv074、XGv302 和 XGv303三株抗体仍具备强效中和能力。进一步研究发现，由于JN.1变异株RBD区L455S突变，仅XGv074抗体对JN.1维持微弱中和活性 ($IC_{50}=2.3$ mg/L)，其中和效价较BA.2.86下降近300倍。因此，深入解析JN.1的免疫逃逸机制，尤其是RBD关键突变对抗体中和活性的影响，对于开发广谱疫苗和新型抗体药物具有重要的科学和临床意义。

1 材料与方法

1.1 Spike蛋白表达与纯化

通过重叠PCR技术，以实验室保存的编码野生型SARS-CoV-2 (GenBank: MN908947) Spike蛋白和RBD质粒为模板，构建了BA.2.86全长Spike蛋白（残基1~1208）的表达载体。为稳定Spike三聚体构象，在BA.2.86 Spike蛋白中引入了6个脯氨酸突变位点 (K817P、A892P、A899P、V942P、K986P和V987P)，将S1/S2弗林蛋白酶切割位点（残基682~685）突变为GSAS序列，并在C端添加了T4 foldon三聚化结构域。随后将重组质粒瞬时转染至悬浮培养的HEK 293F细胞中，在37°C、8% CO₂、130 r/min条件下进行表达培养。转染72 h后收集细胞上清，经浓缩后依次采用链霉亲和素亲和层析和Superdex 6 10/300凝胶过滤层析 (GE Healthcare Life Sciences) 进行纯化，层析柱使用磷酸盐缓冲液 (phosphate-buffered saline, PBS) 平衡。

1.2 抗体表达与Fab片段制备

将XGv074、XGv302和XGv303抗体基因序列经密码子优化后，分别克隆至含有人源化免疫球蛋白G1 (immunoglobulin G1, IgG1) 可结晶片段 (fragment crystallizable, Fc) 的表达载体中，分别构建抗体重链 (heavy chain, HC) 和轻链 (light chain, LC) 的表达质粒。随后，以等摩尔比 (1:

1) 将HC与LC质粒共转染至悬浮培养的哺乳动物HEK 293F细胞中。转染后细胞于37°C、8% CO₂条件下，在恒温摇床 (130 r/min) 中培养5 d以表达抗体。收集细胞培养上清液，采用Protein A亲和层析进行抗体纯化。纯化后的抗体经缓冲液置换，最终保存于PBS中。

为制备Fab，使用Thermo Scientific Pierce™ Fab制备试剂盒处理纯化的全抗体。首先，样本经脱盐柱层析 (例如：PD-10柱) 置换至反应缓冲体系，去除盐分并收集流出组分。随后，将脱盐后的抗体与试剂盒提供的固定化木瓜蛋白酶在37°C下孵育5 h，进行酶切反应。酶切产物经Protein A亲和层析柱分离，特异性去除Fc片段及未切割的完整抗体，收集含有Fab片段的穿透液。最终，Fab片段经透析置换至PBS中。

1.3 生物膜层干涉技术 (BLI)

采用生物膜层干涉技术 (bio-layer interferometry, BLI) 检测抗体与病毒RBD的相互作用。将单克隆抗体 (XGv074、XGv302或XGv303) 通过Protein A生物传感器 (ForteBio) 捕获固定，以PBS和0.02%吐温-20梯度稀释的野生型 (wild type, WT)、BA.2、BA.5、XBB.1.5、BA.2.86及JN.1 RBD蛋白作为分析物进行结合动力学分析。所有结合实验均在25°C条件下进行。原始结合传感数据经ForteBio Octet® Analysis Studio 9.0软件处理，采用1:1 Langmuir结合模型拟合计算结合速率常数 (k_{on})、解离速率常数 (k_{off}) 及平衡解离常数 (K_D)。

1.4 冷冻电镜样品制备与数据收集

将纯化的BA.2.86 Spike蛋白分别与XGv302、XGv074或XGv303的Fab片段按1:1.2的化学计量比混合 (S: Fab)，冰浴孵育10 min形成复合物。取3 μl复合物样品滴加至经辉光放电等离子体处理的300目微孔碳包被金网格 (C-flat CF-1.2/1.3, Protochips) 上，在100%相对湿度环境箱中静置吸附6 s后，使用Vitrobot Mark IV (Thermo Fisher Scientific) 快速玻璃化冷冻至液乙烷混合冷冻剂中。冷冻样品在300 kV Titan Krios G4冷冻电镜 (Thermo Fisher Scientific) 上采集数据，配合Gatan K3 Summit直接电子探测器以超分辨率模式记录图像 (总电子剂量60 e⁻/Å², 32帧/张，单帧曝光时间0.2 s)，散焦范围设置为-1.2至-2.0

μm。使用SerialEM 4.0软件进行自动单颗粒数据采集, 在校准放大倍数22 500×下获得最终像素尺寸1.07 Å的显微图像。

1.5 冷冻电镜数据处理

原始显微图像数据集包含5 187张S-XGv302复合物、1 589张S-XGv074复合物及432张S-XGv303复合物的记录。所有图像预处理均通过RELION 3.0^[6]软件包完成: 使用MotionCor2实施光束诱导运动校正, 并通过Gctf v1.06^[7]计算散焦值与像散参数。颗粒挑选在cryoSPARC v3.2^[8]平台执行, 采用模板无关算法(Template-free picking)分别获得2 494 398个(S-XGv302)、667 768个(S-XGv074)和313 810个(S-XGv303)初始颗粒。经二维分类(2D classification)筛选后, 最终保留982 100个(S-XGv302)、252 504个(S-XGv074)和83 840个(S-XGv303)高质量颗粒用于三维重构。三维重建采用非对称性初始模型生成(AB-Initio reconstruction), 通过异质性细化(heterogeneous refinement)排除构象异质性颗粒后, 最终使用同质性全局优化(homogeneous refinement)结合掩模后处理(masked postprocessing)获得精修密度图。分辨率评估严格遵循金标准准则: 全局分辨率以傅里叶壳层相关系数阈值0.143(FSC=0.143)确定, 并通过ResMap v1.1.4进行局部分辨率验证。

1.6 冷冻电镜结构建模与优化

首先使用UCSF Chimera 1.16^[9]将天然SARS-CoV-2 Spike蛋白三聚体(PDB: 6VYB)及AlphaFold3^[10]预测的XGv302 Fab结构以刚体对接方式拟合至冷冻电镜密度图中; 随后在Coot 0.9.8^[11]中基于序列信息与密度特征手动修正抗原-抗体界面残基、互补决定区(complementarity-determining regions, CDRs)环区及糖基化位点构象; 最终采用Phenix 1.20^[12]进行五轮实空间精修(应用几何约束、Ramachandran权重优化及电子密度匹配), 获得能量最小化的原子模型。

1.7 分子动力学与结合自由能分解

分子动力学模拟采用GROMACS-2021^[13]执行。首先通过Coot优化复合物(WT RBD-XGv302 Fab)原子冲突, 随后构建OPLS-AA力场、TIP3P水分子体系并离子化中和电荷; 模拟流程包括: a. 最陡下降能量最小化(收敛阈值: 力<

1 000 kJ·mol⁻¹·nm⁻¹); b. 分步平衡: 50 ps NVT系综(300 K, Nose-Hoover控温)及100 ps NPT系综(1 bar, Parrinello-Rahman控压); c. 10 ns生产模拟(时间步长2 fs), 应用Verlet截断(半径12 Å)和PME长程静电处理。基于平衡轨迹, 通过gmx-MMPBSA 1.6.4^[14]进行结合自由能残基分解。提取最后50帧构象计算各能量项, 最后绘制RBD上各残基的平均能量和不确定度。

2 结果

2.1 RBD 抗体与 SARS-CoV-2 RBDs亲和力分析

通过BLI实验系统评估了XGv074、XGv302和XGv303三株抗体的结合特性。实验数据显示, 这三种抗体在近亚纳摩尔浓度水平(<3 nmol/L)下均能与WT及Omicron亚系(BA.2和BA.5)的RBD发生强效结合。然而, 其对XBB.1.5和BA.2.86变异株的结合亲和力(K_d 值)显著降低至5~200 nmol/L范围(图1)。值得注意的是, 尽管XGv074与JN.1 RBD的结合亲和力($K_d = 117.5$ nmol/L)较其他毒株明显减弱, 但仍保留一定的中和活性($IC_{50} = 2.3$ mg/L)^[5]。相比之下, XGv302和XGv303则完全丧失了与JN.1 RBD的可检测结合能力。这一结果提示, JN.1突变株的出现使绝大部分抗体发生了逃逸。

2.2 RBD 抗体对 BA.2.86-Spike的冷冻电镜结构

为阐明三种RBD抗体对JN.1变异株的免疫逃逸结构机制, 采用冷冻电镜三维重构技术解析BA.2.86 S蛋白三聚体与XGv074、XGv302及XGv303 Fab片段的复合物结构。通过分别处理5 187、1 589和432张冷冻电镜照片, 成功将XGv302-BA.2.86 S、XGv074-BA.2.86 S和XGv303-BA.2.86 S复合物的结构分辨率提升至3.47 Å、4.04 Å和5.22 Å(图2)。结构分析表明, 三种抗体表位属于RBD上的“A”表位组^[15], 相似表位的代表性抗体还包含LY-CoV016^[16]、BD-515^[17]等。XGv302、XGv074和XGv303与S蛋白三聚体的复合物中两个RBD均呈现“up”构象与两拷贝的Fab结合(图3a), 这与“A”表位抗体仅可及RBD的“up”构象的特征一致。

通过对BA.2.86 RBD和XGv302 Fab复合物进行局部结构优化, 获得了RBD与XGv302 Fab分辨率3.78 Å的精细结构(图3b)。研究发现,

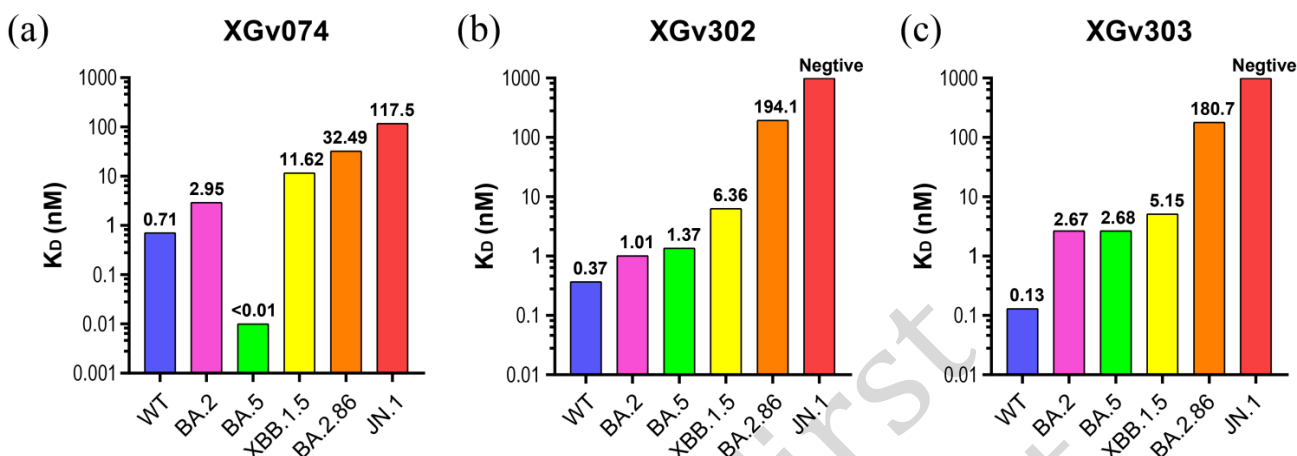


Fig.1 Binding affinity analysis of RBD-targeting antibodies to SARS-CoV-2 RBD variants

Binding affinity of XGv074, XGv302 and XGv303 antibodies to RBD of SARS-CoV-2 variants measured by BLI. Bar charts of dissociation constants (K_D) of XGv074 (a), XGv302 (b), and XGv303 (c) binding to six SARS-CoV-2 RBD variants: wild-type (WT, blue), BA.2 (magenta), BA.5 (green), XBB1.5 (yellow), BA.2.86 (orange), and JN.1 (red).

BA.2.86 RBD的Y421、L455、F456、Y489和Y453残基与抗体HC的Y33、V100、V101和Y102形成关键的疏水相互作用网络。同时，RBD的K460、Y421和Q493残基分别与抗体HC的T56、Y33和Y102形成氢键（图3c）。这些相互作用共同维持了XGv302与BA.2.86 RBD的紧密结合。

序列比对分析显示，XGv074、XGv302和XGv303的LC和HC的CDR区具有高度相似性，这解释了它们对BA.2.86 RBD结合模式的重叠性（图3d, e）。值得注意的是，XGv074的HCDR3区比其他两个抗体多出6个氨基酸，这种结构特征可能赋予其更高的构象柔性，使其能够更好地适应RBD的突变。这一发现为理解XGv074为何能保留对JN.1 RBD的弱结合能力提供了结构基础（图1和图3e）。

2.3 RBD抗体对JN.1逃逸机制分析

结构分析表明，XGv302、XGv303和XGv074均靶向BA.2.86毒株RBD的外周尖端表位，该表位与ACE2结合区域高度重叠（图3d）。基于此结合模式，这三种抗体可通过竞争性抑制病毒-受体

相互作用发挥中和作用（图4a）^[18]。然而，进一步研究发现，JN.1毒株特有的L455S突变选择性地破坏了XGv302的HC与RBD之间的关键疏水相互作用，从而导致JN.1对XGv302产生免疫逃逸（图4b）。

为深入阐明JN.1对XGv302类抗体逃逸的结构基础，采用结合自由能分解方法对BA.2.86 RBD中参与XGv302结合的残基进行了系统分析。定量分析结果显示，在抗体结合界面中，残基415、416、417、456、473、475、476、489、501和505对结合自由能的贡献值主要分布在-3至-2 kcal/mol范围内，表现出相对均衡的能量分布特征。值得注意的是，Y421和L455两个残基显示出显著更高的能量贡献（均小于-3 kcal/mol）（图4c），这一发现从能量学角度证实了这两个位点在抗体-RBD相互作用中的关键作用。特别需要指出的是，L455S突变通过特异性破坏这一关键能量贡献位点，直接导致XGv302类抗体中和活性的丧失，这为理解JN.1变异株的免疫逃逸机制提供了重要的结构生物学依据。

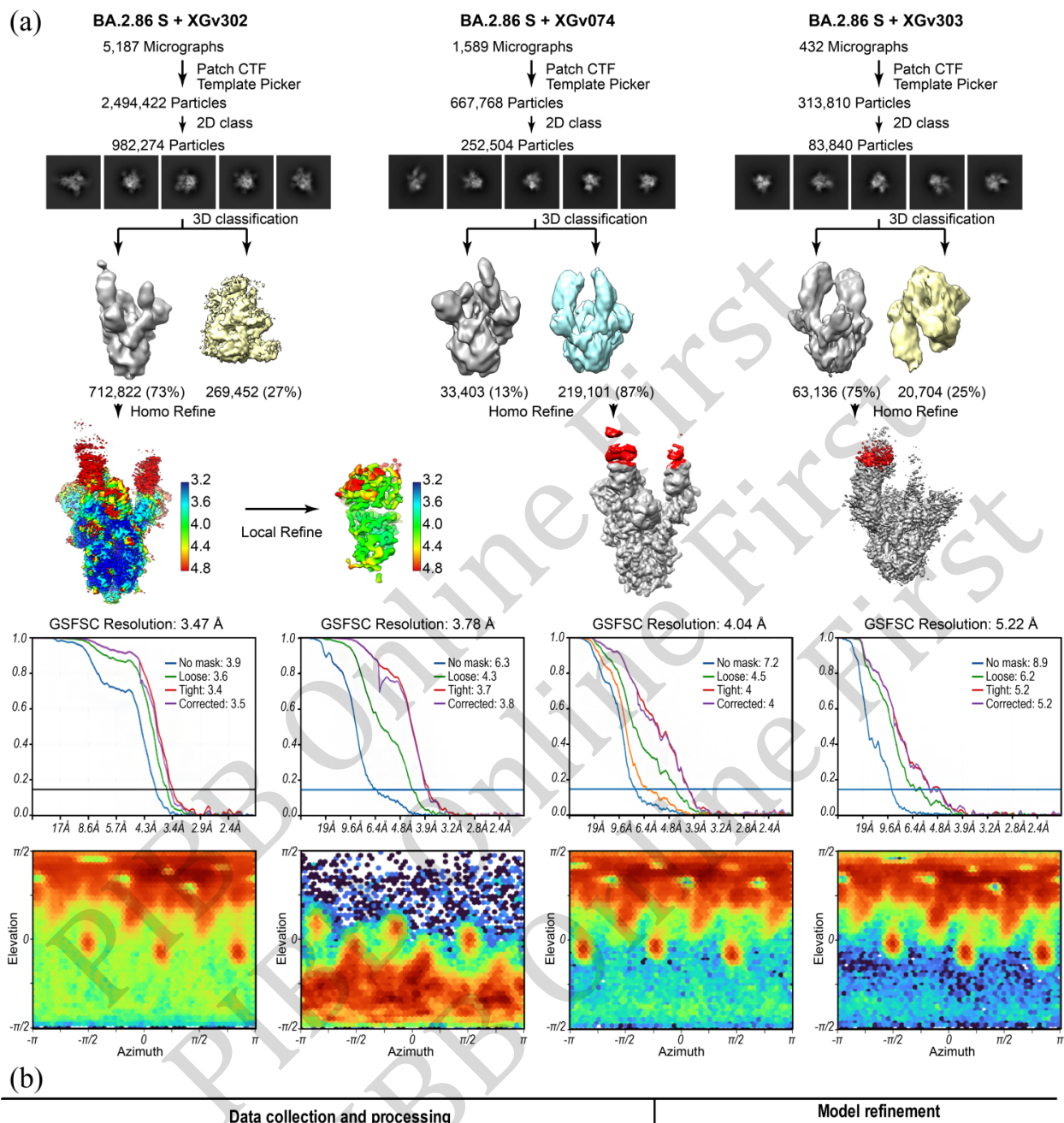


Fig. 2 Cryo-EM data of BA.2.86 S-trimer in complex with neutralizing antibodies

(a) Cryo-EM single-particle analysis of BA.2.86 S-trimer in complex with neutralizing antibodies. Flowcharts of reconstructed densities of BA.2.86 S-trimer in complex with XGv302(left), XGv074 (middle) and XGv303 (right) are shown. Resmaps of Cryo-EM density of BA.2.86 S-trimer and RBD in complex with XGv302 are shown, and Fab XGv074 and XGv303 are highlighted in their final low resolution density maps. FSC curves of reconstructed densities of BA.2.86 S-trimer in complex with XGv302 (Overall and Interface), XGv074 (Overall) and XGv303 (Overall) are shown. The scatter plot shows the distribution of Euler angles of the particles included in the final reconstruction. Each point represents a specific projection direction. The color intensity of the points indicate the relative abundance of particles at that orientation. (b) Cryo-EM data collection and atomic models refinement statistics.

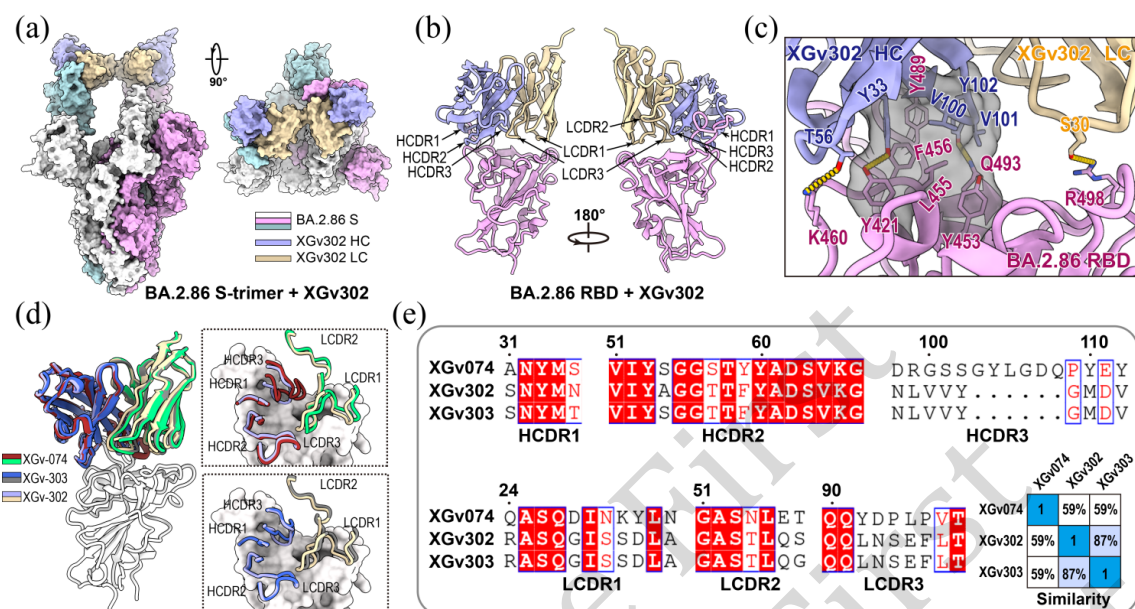


Fig.3 Structural characterization of RBD–targeting antibodies interactions with BA.2.86 spike and RBD

(a) Surface representation of XGv302 Fab in complex with BA.2.86-S-trimer. The trimeric spike protein of BA.2.86 is colored in white, cyan, and pink (representing each protomer chain). XGv302 HC is colored in light purple and XGv302 LC is colored in wheat. (b) Cartoon representation of BA.2.86 RBD in complex with XGv302. The same color scheme as (a) was used. (c) Detailed view of the binding interface between BA.2.86 RBD and XGv302 Fab. The grey surface represents the hydrophobic pocket and yellow dashed lines represent hydrogen bonds. (d) Left: superimposition of RBD in complex with XGv074, XGv302 and XGv303. Right: superimposition of RBD in complex with six CDRs between XGv074 and XGv302 (top), and six CDRs between XGv303 and XGv302 (bottom). XGv302 HC and LC are colored in light purple and wheat, respectively. XGv074 HC and LC are colored in brown and spring, respectively. XGv303 HC and LC are colored in blue and gray, respectively. (e) Sequence alignment of CDRs for XGv074, XGv302 and XGv303 antibodies and the corresponding sequence identity matrix of CDRs.

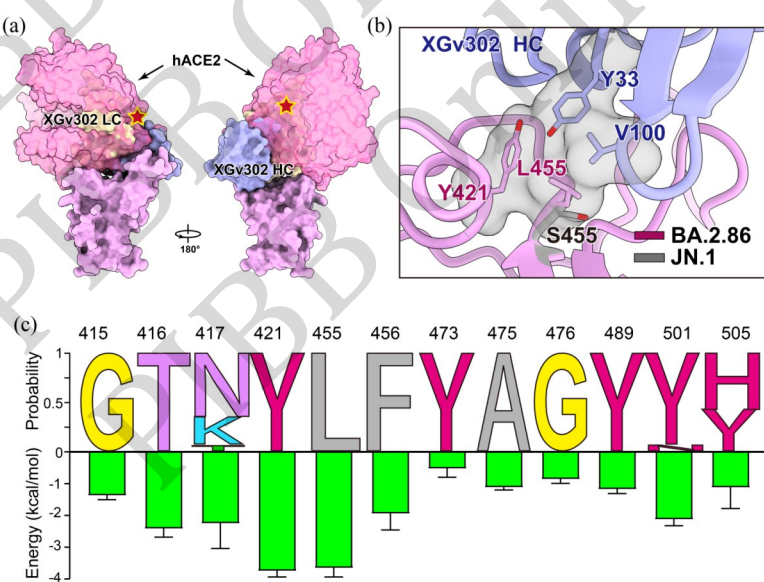


Fig.4 Structural Basis for RBD–Targeting Antibody Evasion by the JN.1 Variant

(a) XGv302 neutralizing mechanism. The BA.2.86 RBD and XGv302 Fab are shown as surface. BA.2.86 RBD is colored in pink; hACE2 is colored in hot pink; XGv302 HC and LC is colored in light purple and wheat. Steric clash is marked as red stars. (b) Structural analysis of JN.1 RBD elucidating the mechanism of XGv302 evasion. All structures are shown as ribbon with the key residues shown with sticks. The same color scheme as (a) was used. (c) Weblogo plot of conservation and bar chart of average binding free energy estimated by gmx-MMPBSA of all epitopes of XGv302. Top panel: Sequence logo plot depicting conservation of XGv302 epitope residues across 26 SARS-CoV-2 lineages (B.1; B.1.1.7; B.1.351; P.1; B.1.617.2; B.1.617.1; B.1.427; B.1.525; B.1.526; C.37; BA.1; BA.2; BA.5; BA.2.12.1; BA.2.75; BQ.1; BQ.1.1; XBB; XBB.1.5; XBB.1.16; CH.1.1; XBB.1.9; XBB.1.9.1; XBB.2.3; XBB.1.5.44; BA.2.86). Bottom panel: Quantitative binding free energy contributions (kcal/mol) of individual WT RBD residues.

3 讨论

本研究通过综合运用结构生物学、生物物理学和病毒学方法,系统阐明了SARS-CoV-2 JN.1变异株对广谱中和抗体的逃逸机制。研究结果表明,JN.1变异株通过RBD区关键位点突变,特别是L455S突变,实现了对绝大多数中和抗体的逃逸,这一发现为理解当前流行株的免疫逃逸特性提供了重要见解。

冷冻电镜结构揭示,三种抗体均识别位于RBD尖端、与ACE2结合区域高度重叠的保守表位。这种结合模式解释了它们对BA.2.86之前多数毒株的广谱中和能力。然而,在JN.1中出现的L455S突变选择性破坏了XGv302与RBD之间的关键疏水相互作用,导致其完全失去对JN.1的结合和中和功能。结合自由能分解结果进一步佐证了这一机制:Y421和L455是XGv302结合界面的两个主要能量“热点”残基,而L455S突变直接破坏了其中一个关键能量贡献点,从而引起结构与能量层面的联动性损伤。这为我们理解单点突变如何造成抗体功能“断崖式”下降提供了分子机制解释。

值得关注的是,XGv074尽管与XGv302和XGv303在CDR序列和表位识别模式上高度相似,但其保留了对JN.1的弱结合能力和中和活性。结构分析显示,XGv074具有更长且富含柔性残基的HCDR3结构,这可能增强了其对RBD构象变化的适应性。由于BA.2.86 S蛋白三聚体与XGv074 Fab整体分辨率仅为4.04 Å,无法进一步通过局部优化确定RBD与XGv074 Fab的高分辨界面结构,界面分辨率不足限制了我们通过抗体结构的密度或B因子进行进一步的柔性确认。即便如此,我们推测,这种“构象柔性”可能赋予其在高突变背景下仍保留部分识别能力的结构优势。类似现象也在人类免疫缺陷病毒(Human Immunodeficiency Virus,HIV)广谱中和抗体研究中被广泛观察。以PGT135为代表的HIV广谱抗体通过一个长度为18的HCDR3环结构与包膜蛋白结合(人类HCDR3的平均长度为13个残基),形成更深的抗原结合口袋,以穿透HIV包膜蛋白表面的糖基化屏障,从而识别包膜蛋白上进化保守的“脆弱位点”,发挥广谱中和的效果^[19]。这提示HCDR3长度和柔性在识别快速进化病毒中扮演重要角色。

综上所述,BA.2.86及其子代JN.1的RBD变异不仅改变了抗原表位的空间构象,同时通过破坏抗

体-抗原之间的关键疏水和氢键网络,实现对主流A类RBD抗体的有效逃逸。我们的研究强调了在广谱抗体筛选与疫苗设计过程中,需重点关注表位能量分布、抗体构象适应性以及突变耐受能力等因素。未来的广谱抗体开发策略可考虑引入高柔性的HCDR3区域,或采用混合表位识别模式以提升抗突变能力。此外,结合结构生物学与计算能量分析方法,将为预测潜在逃逸突变、设计预应对性抗体库提供新的方向。

4 结论

SARS-CoV-2 JN.1 变异株通过 RBD 区关键 L455S 突变破坏抗体结合的关键疏水网络,导致广谱抗体 XGv302 和 XGv303 逃逸,但 XGv074 因 HCDR3 构象柔性仍保留部分中和活性。研究为广谱抗体设计提供新策略,提示需同时靶向保守表位能量热点并增强抗体 CDR 结构柔性,以应对病毒持续进化带来的免疫逃逸挑战。

参 考 文 献

- [1] Jian F, Wang J, Yisimayi A, et al. Evolving antibody response to SARS-CoV-2 antigenic shift from XBB to JN.1. *Nature*, 2025, **637**(8047): 921-929
- [2] Lan J, Ge J, Yu J, et al. Structure of the SARS-CoV-2 spike receptor-binding domain bound to the ACE2 receptor. *Nature*, 2020, **581**(7807): 215-220
- [3] Li L, Shi K, Gu Y, et al. Spike structures, receptor binding, and immune escape of recently circulating SARS-CoV-2 Omicron BA.2.86, JN.1, EG.5, EG.5.1, and HV.1 sub-variants. *Structure*, 2024, **32**(8): 1055-1067.e6
- [4] Yang S, Yu Y, Xu Y, et al. Fast evolution of SARS-CoV-2 BA.2.86 to JN.1 under heavy immune pressure. *Lancet Infect Dis*, 2024, **24**(2): e70-e72
- [5] Zhu Q, Liu P, Liu S, et al. Enhancing RBD exposure and S1 shedding by an extremely conserved SARS-CoV-2 NTD epitope. *Signal Transduct Target Ther*, 2024, **9**: 217
- [6] Scheres S H W. RELION: Implementation of a Bayesian approach to cryo-EM structure determination. *J Struct Biol*, 2012, **180**(3): 519-530
- [7] Zhang K. Gctf: real-time CTF determination and correction. *J Struct Biol*, 2016, **193**(1): 1-12
- [8] Punjani A, Rubinstein J L, Fleet D J, et al. cryoSPARC: algorithms for rapid unsupervised cryo-EM structure determination. *Nat Methods*, 2017, **14**(3): 290-296
- [9] Pettersen E F, Goddard T D, Huang C C, et al. UCSF Chimera—a visualization system for exploratory research and analysis. *J Comput Chem*, 2004, **25**(13): 1605-1612
- [10] Abramson J, Adler J, Dunger J, et al. Accurate structure prediction

- of biomolecular interactions with AlphaFold 3. *Nature*, 2024, **630** (8016):493-500
- [11] Emsley P, Cowtan K. *Coot*: model-building tools for molecular graphics. *Acta Crystallogr D Biol Crystallogr*, 2004, **60**(12): 2126-2132
- [12] Adams P D, Afonine P V, Bunkóczki G, et al. PHENIX: a comprehensive Python-based system for macromolecular structure solution. *Acta Crystallogr D Biol Crystallogr*, 2010, **66** (Pt 2):213-221
- [13] Van Der Spoel D, Lindahl E, Hess B, et al. GROMACS: fast, flexible, and free. *J Comput Chem*, 2005, **26**(16): 1701-1718
- [14] Valdés-Tresanco M S, Valdés-Tresanco M E, Valiente P A, et al. gmx_MMPBSA: a new tool to perform end-state free energy calculations with GROMACS. *J Chem Theory Comput*, 2021, **17** (10):6281-6291
- [15] Cao Y, Yisimayi A, Jian F, et al. BA.2.12.1, BA.4 and BA.5 escape antibodies elicited by Omicron infection. *Nature*, 2022, **608** (7923):593-602
- [16] Shi R, Shan C, Duan X, et al. A human neutralizing antibody targets the receptor-binding site of SARS-CoV-2. *Nature*, 2020, **584**(7819): 120-124
- [17] Cao Y, Yisimayi A, Bai Y, et al. Humoral immune response to circulating SARS-CoV-2 variants elicited by inactivated and RBD-subunit vaccines. *Cell Res*, 2021, **31**(7): 732-741
- [18] Jia Z, Wang K, Xie M, et al. A third dose of inactivated vaccine augments the potency, breadth, and duration of anamnestic responses against SARS-CoV-2. *Protein Cell*, 2024, **15**(12): 930-937
- [19] Kong L, Lee J H, Doores K J, et al. Supersite of immune vulnerability on the glycosylated face of HIV-1 envelope glycoprotein gp120. *Nat Struct Mol Biol*, 2013, **20**(7): 796-803

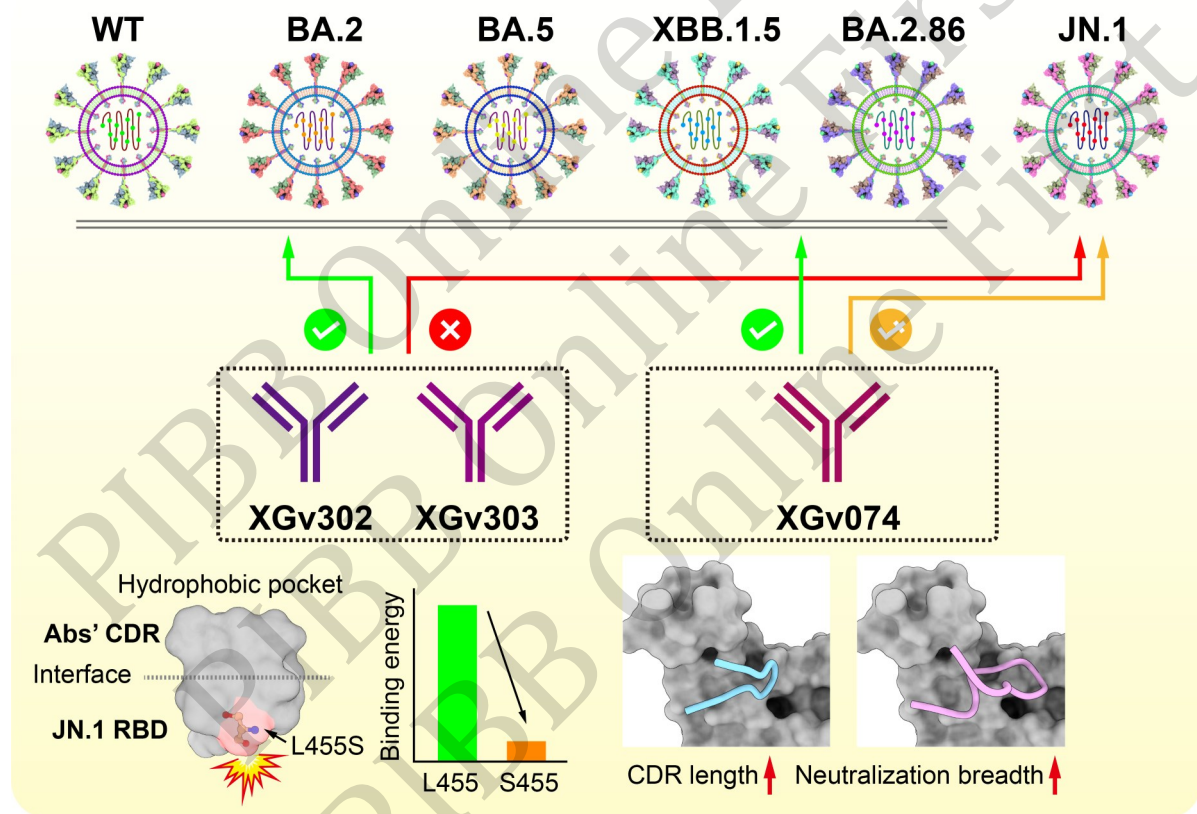
Mechanisms of Immune Evasion by The SARS-CoV-2 JN.1 Variant Against Broadly Neutralizing Antibodies*

XIE Jia-Wen¹⁾, LIU Tian-Ci²⁾, GUO Meng-Tian²⁾, FENG Lu-Lu²⁾, SUN Ming-Chen²⁾,
LIU Pan²⁾, ZHU Qian-Hui^{2)***}

(¹)College of Life Sciences, Beijing Normal University, Beijing 100875, China;

(²)State Key Laboratory of Biomacromolecules, Institute of Biophysics, Chinese Academy of Sciences, Beijing 100101, China)

Graphical abstract



Abstract Objective With the continuous evolution of severe acute respiratory syndrome-coronavirus 2 (SARS-CoV-2) Omicron subvariants, particularly the emergence of BA.2.86 and its descendant JN.1, the efficacy of current neutralizing antibodies has faced substantial challenges. The JN.1 variant, noted for its pronounced immune evasion capacity, has rapidly become the globally dominant strain. Elucidating its escape mechanisms is therefore essential to guide the development of next-generation broad-spectrum vaccines and neutralizing antibody therapeutics. This study aimed to investigate the immune evasion mechanisms of JN.1 against broadly neutralizing antibodies, focusing on the effects of key receptor-binding domain (RBD) mutations on antibody binding and neutralization, thereby providing theoretical support for countering ongoing viral evolution.

Methods We employed a multidisciplinary approach to systematically assess the binding and neutralizing activities of three broad-spectrum neutralizing antibodies (XGv074, XGv302, and XGv303) against BA.2.86 and

JN. 1. Binding affinities (KD values) of antibodies to variant RBDs were determined using bio-layer interferometry (BLI). Cryo-electron microscopy (cryo-EM) was used to resolve the structure of the BA.2.86 Spike trimer in complex with antibody antigen-binding fragments (Fab), achieving a resolution of 3.47 Å for the BA.2.86 S-trimer bound to XGv302. Molecular dynamics simulations and binding free-energy decomposition were conducted to quantify the contributions of key mutations at the antibody – RBD interface. Additionally, sequence alignment and structural modeling were performed to evaluate the role of conformational flexibility in the antibody heavy-chain complementarity-determining region 3 (HCDR3) in mediating tolerance to mutations.

Results Experimental data showed that XGv074, XGv302, and XGv303 retained neutralizing activity against BA.2.86 but exhibited markedly reduced binding to JN. 1, with only XGv074 maintaining weak neutralization ($IC_{50} = 2.3$ mg/L). Cryo-EM structures revealed that all three antibodies targeted the RBD tip, overlapping with the ACE2-binding region. The JN. 1-specific L455S mutation disrupted the hydrophobic interaction network between XGv302 and the RBD (involving key residues such as Y421 and L455), resulting in complete loss of neutralization. Binding free-energy decomposition further identified L455 and Y421 as energetic hotspots ($\Delta G < -3$ kcal/mol), with the L455S mutation directly impairing antibody binding. XGv074, owing to greater conformational flexibility in its HCDR3 region, partially tolerated the mutation and retained weak binding. Molecular dynamics simulations showed that the L455S mutation not only eliminated the energetic contribution of this residue but also caused a concurrent decrease in binding free energy of neighboring residues, thereby reducing overall interface stability. **Conclusion** The JN.1 variant escapes broad-spectrum neutralizing antibodies primarily through the L455S mutation in the RBD, which disrupts energetic hotspots and remodels the antibody-binding interface. Antibody conformational flexibility enhances adaptability to such mutations, providing new insights for broad-spectrum antibody design. These findings highlight the critical roles of epitope energy distribution and antibody flexibility in maintaining neutralization breadth, offering essential guidance for the rational design of next-generation vaccines and antibody therapeutics: specifically, by targeting conserved energetic hotspots while enhancing CDR flexibility to counter immune evasion driven by viral evolution.

Key words SARS-CoV-2, BA. 2.86, JN. 1, neutralizing antibodies, cryo-electron microscopy, neutralization mechanism, immune evasion mechanism

DOI: 10.3724/j.pibb.2025.0336 **CSTR:** 14.32369.pibb.20250336

* This work was supported by a grant from National Key Research and Development Program (2018YFA0900801).

** Corresponding author.

Tel: 86-10-64889939, E-mail: zhuqianhui@ibp.ac.cn

Received: July 15, 2025 Accepted: August 18, 2025